

Surface oxygen vacancies in gold based catalysts for CO oxidation

Cite this: *RSC Adv.*, 2014, 4, 13145

F. Romero-Sarria,^{*a} J. J. Plata,^b O. H. Laguna,^a A. M. Márquez,^b M. A. Centeno,^a J. Fdez Sanz^b and J. A. Odriozola^a

Experimental catalytic activity measurements, diffuse reflectance infrared Fourier spectroscopy, and density functional theory calculations are used to investigate the role and dynamics of surface oxygen vacancies in CO oxidation with O₂ catalyzed by Au nanoparticles supported on a Y-doped TiO₂ catalyst. Catalytic activity measurements show that the CO conversion is improved in a second cycle of reaction if the reactive flow is composed by CO and O₂ (and inert) while if water is present in the flow, the catalyst shows a similar behaviour in two successive cycles. DRIFTS-MS studies indicate the occurrence of two simultaneous phenomena during the first cycle in dry conditions: the surface is dehydroxylated and a band at 2194 cm⁻¹ increases (proportionally to the number of surface oxygen vacancies). Theoretical calculations were conducted in order to explain these observations. On one hand, the calculations show that there is a competition between gold nanoparticles and OH to occupy the surface oxygen vacancies and that the adsorption energy of gold on these sites increases as the surface is being dehydroxylated. On the other hand, these results evidence that a strong electronic transfer from the surface to the O₂ molecule is produced after its adsorption on the Au/TiO₂ perimeter interface (activation step), leaving the gold particle in a high oxidation state. This explains the appearance of a band at a wavenumber unusually high for the CO adsorbed on oxidized gold particles (2194 cm⁻¹) when O₂ is present in the reactive flow. These simultaneous phenomena indicate that a gold redispersion on the surface occurs under reactive flow in dry conditions generating small gold particles which are very active at low temperature. This fact is notably favoured by the presence of surface oxygen vacancies that improve the surface dynamics. The obtained results suggest that the reaction mechanism proceeds through the formation of a peroxo-like complex formed after the electronic transfer from the surface to the gas molecule.

This article can be cited before page numbers have been issued, to do this please use: F. Romero-Sarria, J. Plata, O. H. Laguna, A. Márquez, M. A. Centeno, J. Fernández Sanz and J. A. Odriozola, *RSC Adv.*, 2014, DOI: 10.1039/C3RA46662K.

Received 13th November 2013
Accepted 25th February 2014

DOI: 10.1039/c3ra46662k

www.rsc.org/advances

Introduction

In the field of catalysis by gold, CO oxidation is among the most studied reactions due to the high activity of gold-based catalysts in this process.^{1–6} CO abatement from the atmosphere or from gas streams feeding fuel cells is a key factor in the development of new technologies for environmental applications.^{7–9} Therefore, aspects related to the mechanism of the CO oxidation reaction^{10–14} on gold-based catalysts such as gold particle size,^{15–18} gold oxidation state,^{19,20} the role of the catalytic support^{18,21,22} and the presence of water in the reactive flow¹¹ have been widely treated in literature. Some authors observed that gold oxidized species are the most active ones showing also the highest thermal stability.²³ However, *in situ* studies showed that metallic gold is the only species on the catalyst surface under reactive conditions.²⁴ According to Minato *et al.*,²⁵ the presence of sites with high

electronic density on the surface is essential to the occurrence of the CO oxidation since the electronic transfer from these sites to the oxygen 2π* antibonding orbital is necessary for its activation (rate-determining step). These authors observed the presence of gold species in different oxidation states and the modification of them during the reaction. A general agreement exists on a Langmuir–Hinshelwood mechanism, in which, both the oxygen and the CO are adsorbed on the surface to react in a further step giving rise to CO₂. The sites for the CO adsorption are well defined: gold nanoparticles.²⁶ However, the sites for the oxygen activation are uncertain because they depend on the nature of the catalytic support.²⁷ Analyzing the sites on which the oxygen is activated, Schubert *et al.*²⁸ classified the supports as “inert” and “active”. Generally, it is considered that an inert support does not participate in the reaction and both oxygen and CO adsorption proceed on the gold nanoparticles. In contrast, “active” supports provide sites for the oxygen activation, generating active species to the oxidation.²⁹ This classification is based on the redox properties of the supports, being the reducible ones called “actives” and the non-reducible ones “inerts”. On this basis, gold particle size is a determining parameter in the reactivity of gold supported on

^aDepartamento de Química Inorgánica and Instituto de Ciencia de Materiales de Sevilla, Centro Mixto Universidad de Sevilla - CSIC, Avda. Américo Vespucio, 49, 41092 Sevilla, Spain. E-mail: francisca@icmse.csic.es

^bDepartamento de Química Física, Facultad de Química, Universidad de Sevilla, C/ Profesor García González, s/n, 41012 Sevilla, Spain

“inert” materials given that the adsorption proceeds on the metallic particles, while its influence should be less important for active supports, in which, the role of the support becomes more important. More recent works propose that the presence of oxygen vacancies in the support (reducible or irreducible) has also an important influence on the catalytic activity in CO oxidation. Studies of this reaction using an inert support (calcium hydroxyapatite) evidenced that the creation of structural oxygen vacancies by removal of hydroxyl/carbonate groups from the support structure increases the CO conversion rate.³⁰ In this case, the interaction of gaseous O₂ with the oxygen vacancies created in the support, generates peroxide species that are responsible for the high CO conversion detected at room temperature.

The effect of the oxygen vacancies has also been observed in reducible supports. Hernández *et al.*³¹ prepared and studied catalytic supports by doping ceria with variable amounts of europium. Raman studies evidenced that the isomorphous replacement of Ce⁴⁺ ions by Eu³⁺ cations resulted in a solid solution in which, oxygen vacancies are created in order to maintain the charge equilibrium. An estimate of the oxygen vacancies density revealed that it is proportional to the amount of doping element. The oxygen vacancy density and the measured CO conversion correlate fairly well. Moreover, Raman analysis of the supports and catalysts shows that surface oxygen vacancies disappear on adding gold to the support, suggesting that this type of defect acts as nucleation sites for gold, as previously reported by other authors.³²

Modifications of the CO conversion in successive reaction cycles have also been associated to the surface dynamics promoted by the presence of oxygen vacancies.³³ It has been observed that this promotion is higher when the oxygen vacancies are located on the surface of the solid.³⁴ Therefore, knowledge about the role of surface oxygen vacancies in the mechanism of the CO oxidation reaction is a key point in the design of new active catalysts for environmental applications. However, some aspects related to the surface dynamics, intermediate of reaction and the influence of water on the CO conversion are still unexplored in solids containing oxygen vacancies.

Based on this interest, supports consisting in titania doped with yttrium were prepared and characterized in a previous work.³⁴ In brief, XRD analysis of the solids calcined at 300 °C evidenced that anatase is the only crystalline phase present if the yttrium content ranges from 0 to 11 wt%. *In situ* studies showed that the anatase to rutile phase transformation is produced at temperatures higher than 500 °C when yttrium is present. DFT calculations suggested that Y is mainly located on the surface of the solid in such a way that the oxygen vacancies created by doping are also on the surface. Catalytic results demonstrated the positive effect of the yttrium content on the CO conversion at low temperature, being the most active solid that with the higher amount of yttrium. This fact was explained by the role of the oxygen vacancies as gold nucleation centres: a high number of oxygen vacancies on the surface induces the formation of very small gold particles with high activity at room temperature, as previously reported in literature.⁴ Starting from these observations, measurements of the catalytic activity in successive cycles of reaction in presence and absence of water in

the reactive flow, DRIFTS-MS studies and DFT calculations are combined in the present work to investigate the role of the surface oxygen vacancies in the reaction mechanism, the effect of the water and if possible, the most active gold oxidation state.

Results and discussion

TiO₂-Y (6 wt%) support was tested in the CO oxidation reaction. The obtained conversions were lower than 1% at 300 °C, but the gold incorporation to the solid notably improves the CO conversion. Light-off curves in two successive cycles of reaction in dry (3.4% CO and 21% O₂, balanced by He) and wet (3.4% CO, 21% O₂ and 2% H₂O balanced by He) conditions are presented in Fig. 1.

In dry conditions, the CO conversion at 30 °C is around 3% in the first cycle and it increases to about 10% in the second one. At higher temperatures, the CO conversions measured during the second cycle decreases in relation to that obtained for the first one. According to Simakov *et al.*,³⁵ the activity at low temperature is due to the presence of Au_n^{δ+} or Au⁰ clusters with diameter smaller than 1 nm, while the conversion of CO at high temperature is associated to the presence of gold nanoparticles with sizes between 2 and 20 nm. Considering these ideas, the light-off curves shown in Fig. 1 suggest that modifications of the gold particle size and/or gold oxidation state are produced during the first cycle of reaction (thermal treatment under dry flow).

Fig. 1 also includes the light-off curves obtained in wet conditions. In this case, the CO conversion in all the range of temperature appreciably decreases if compared to dry conditions, meaning that water inhibits the reaction in some extent. Studies by Daté *et al.*³⁶ pointed out that the presence of water in the reactive flow has a positive effect if the concentration is lower than 200 ppm, while a higher amount of moisture in the flow results in a decreasing of the CO conversion due to the blockage of the active sites on the surface. In our case, the water amount is higher than 200 ppm and a negative effect is expected, as observed in Fig. 1. No modifications are detected in the second cycle of reaction regarding the first one, meaning that the solid is not strongly modified under wet conditions. That is, the presence of water could inhibit the creation of gold particles actives at low temperature by modification of the oxidation state and/or particle size, as observed in absence of water.

In operando DRIFTS-MS studies were conducted in order to get insight into the modifications observed in dry conditions. At the beginning of the reaction (room temperature), the formation

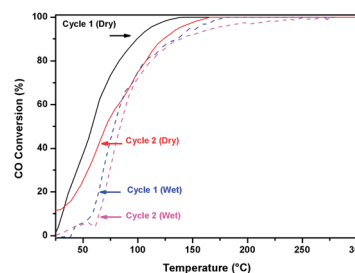


Fig. 1 Light-off curves for two successive cycles of reaction in dry and wet conditions using the AuTiY₆ catalyst.

of monodentate carbonate species (bands around 1504 and 1400 cm^{-1}) was detected on the surface.³⁷ The intensity of these bands decreased with the temperature until their practical disappearance at about 200 °C.

In the carbonyls region only one band at 2194 cm^{-1} was detected at the highest temperature (300 °C). A band at a similar frequency has been attributed to CO adsorbed on Ti^{4+} in Au/ TiO_2 catalysts at -183 °C and at room temperature.³⁸ The vanishing of this band at higher temperatures evidenced the low thermal stability of these species.^{38,39} Risse *et al.*⁴⁰ prevents against tempting to assign high frequency CO bands to the presence of point defects on the surface, since point defects on ionic oxides, results in negatively charged Au particles exhibiting a red shift of the CO stretching band by 40–100 cm^{-1} depending on particle size.⁴¹ Moreover, a band at 2195 cm^{-1} was observed for $\text{Au}^+(\text{CO})$ clusters isolated in superacid matrices.⁴² Hadjiivanov and Vayssilov³⁹ reports that gold forms non-classical ionic carbonyls, $\text{Au}^{\delta+}\text{-CO}$ species, characterized by IR stretching modes at 2190–2176 cm^{-1} . Considering the composition of our catalyst, only Ti^{4+} and gold species are available to adsorb CO giving a band in the 2200–2000 cm^{-1} region. Given that $\text{Ti}^{4+}\text{-CO}$ species are unstable at temperatures higher than room temperature, the assignment of the 2194 cm^{-1} band to CO adsorbed on gold species in high oxidation state seems to be preferable,⁴³ even if the typical band of CO adsorbed on oxidized gold species are usually observed at lower wavenumbers.³² This attribution will be discussed considering the results from DFT calculations.

When the temperature in the reaction chamber is constant (300 °C), and the steady state seems to be attained, some modifications in the carbonyls and hydroxyls regions are still observed. In order to properly detect these modifications, the spectrum of the surface recorded once the temperature reached 300 °C is subtracted from the spectrum after 40 minutes at 300 °C (under reactive flow). Two simultaneous modifications are observed, Fig. 2: the intensity of the band at 2194 cm^{-1} increases and that of the feature at 3660 cm^{-1} decreases.

This last band corresponds to hydroxyls groups in adjacent unit cells of the titania surface.⁴⁴ This evidences the surface dehydroxylation, probably due to the kinetic of the process starting at 300 °C and strongly influenced by the atmosphere⁴⁵ and/or by reaction.⁴⁶ Assuming that the band at 2194 cm^{-1} is due to CO adsorbed on gold species, the observed increasing in the intensity with time has to be related to an increase in the

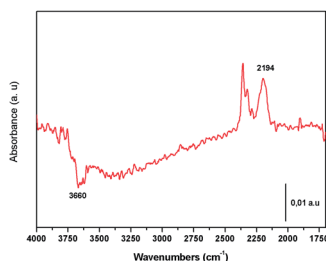


Fig. 2 Modifications of the surface after 40 minutes at 300 °C under reactive flow (difference spectrum taking as reference the spectrum of the surface after 0 min at 300 °C under reactive flow).

number of gold adsorption sites, which may only be explained if a gold redispersion on the surface proceeds in these conditions. It is worth noting that gold nanoparticles cannot be seen in high resolution TEM images (not shown) of the catalyst after reaction which supports the gold redispersion process. Therefore, we can propose that at 300 °C, under the reaction atmosphere, the dehydroxylation of the surface is simultaneous to the gold redispersion on the surface. The high wavenumber observed suggests that the gold species are in a high oxidation state.

Gold redispersion has been previously observed, for example, in an Au/ CeO_2 catalyst during the reduction with CO at 300 °C, and it was related with the creation and mobility of oxygen vacancies on the surface.³³ In order to verify this idea, and to find the relation existing between the density of oxygen vacancies and the gold redispersion, the area of the band at 2194 cm^{-1} was represented as a function of the time (temperature, flow and CO conversion are constants) for catalysts containing different amounts of doping agent and they are shown in Fig. 3.

The evolution of these curves represents the modification of the relative number of gold sites on the surface with time and therefore, the slopes of these curves give a semi quantitative measure of the surface gold redispersion rate. It is observed that the redispersion rate is higher as the Y load increases, suggesting that this phenomenon (gold redispersion simultaneous to the surface dehydroxylation in all the cases) is strongly related to the surface density of oxygen vacancies. Since a gold redispersion implies smaller gold particles, after the first cycle of reaction, a more active catalyst at low temperatures should be obtained, as observed in Fig. 1. In relation to the water effect, it must be considered that the presence of water in the reactive flow hampers the surface dehydroxylation by modification of the equilibrium adsorption–desorption between the surface and the gas phase. This explains the lower activity observed in wet conditions (Fig. 1).

In summary, experimental results in steady state conditions show the presence of a band attributed to CO adsorbed on gold species in high oxidation state, at a wavenumber unusually high (2194 cm^{-1}) that increases with the surface dehydroxylation degree at a rate proportional to the Y content.

In order to explain the simultaneous processes and the attribution of the band at 2194 cm^{-1} , theoretical calculations were carried out.

Results from a previous paper⁴ have shown that the adsorption of a single Au atom on hydrated models of the Y-doped anatase (101) surface is exothermic by -0.47 eV if the gold atom

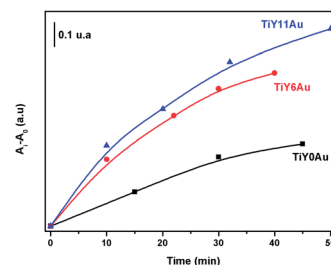


Fig. 3 Evolution of the area of the band at 2194 cm^{-1} with time for catalysts containing different amounts of Y (catalysts under reactive dry flow at 300 °C).

sits on the surface and -0.42 eV if the gold atom is adsorbed on an oxygen vacancy (O_v) site, displacing an hydroxyl group to a surface Ti site. The small difference between these two possibilities means that, at least from a thermodynamic viewpoint, there should be a competition between the gold atoms and the OH to occupy the surface O_v sites. Moreover, when the surface gets dehydroxylated, the adsorption energy of a single gold atom at the O_v site increases notably to -0.81 eV. While the numbers are different, the tendency is the same when small Au_4 nanoparticles (NP) are considered: the adsorption energies on the hydroxylated surface are similar $-1.96/-2.01$ eV (when gold/OH occupies the O_v site) and increases (to -2.39 eV) for Au_4 adsorption on the O_v site in a dehydrated surface model. These data endorse the previous experimental interpretation at a microscopic level: during the reaction cycle, and as the system temperature is increased, the surface gets dehydroxylated, more O_v sites are exposed and the gold particles diffuse to occupy these newly available and thermodynamically more stable sites. Hence, the energetics of Au and Au_4 NP on the catalyst surface, as obtained in our DFT calculations, is consistent with the experimentally observed gold redispersion over the dehydroxylated support surface.

However, these same theoretical calculations predict a surface to Au/ Au_4 charge transfer upon adsorption at the O_v site. These results are clearly inconsistent with the experimental observation of a gold species in a high oxidation state (as concluded from the 2194 cm^{-1} CO vibrational frequency) and a closer investigation of the microscopic mechanism of the CO oxidation reaction is in order. Since experiments are carried out in a flow containing 20% O_2 and 3.4% CO, the adsorption of both molecules on the surface were studied.

Table 1 collects the results (adsorption energies, Bader charge analysis, CO bond distance, and CO stretch vibrational frequency) for CO adsorption on Au_4 NP supported on the different considered models of the anatase (101) surface. In all cases, different coordination geometries were considered and only the results corresponding to the most stable configuration are presented. As expected, CO always acts as a monodentate ligand and preferentially binds undercoordinated Au atoms. Adsorption energies are moderately high, from -1.30 eV to -1.47 eV, but increases to -1.84 eV in the hydrated model of the Y-doped TiO_2 surface when the gold NP sits on the O_v site.

In all cases, the computed Bader charge for the CO molecule is less than $0.001|e|$. This means that the amount of σ -donation is equal to the π -backdonation. The small increase in the CO

bond distance ($0.006\text{--}0.011\text{ \AA}$) shows that this latter contribution to the Au–CO bond is small, as could be expected in the case of an $Au^{\delta+}$ –CO complex.

In fact, the computed Bader charges for the Au atom bonded to the CO show that, while initially the atom is negatively charged or neutral, after CO adsorption the Au atom is always positively charged. The computed CO stretch wavenumbers agree with the presence of a positively charged gold species. In all cases, the computed wavenumbers are between 1960 cm^{-1} and 2192 cm^{-1} , the computed CO stretch frequencies for isolated Au–CO and Au^+ –CO complexes with the same theoretical approach.⁴⁷ Closer examination of the Bader charge analysis shows that, upon CO adsorption, there is a charge reorganization inside the Au NP: the σ lone pair of the CO molecule polarizes the electron density of the Au NP towards the Au atoms that are in contact with the support surface, while the Au atom bonded to the CO molecule remains positively charged. This charge reorganization, and the higher electron density in the Au atoms that sit near the O_v sites, has an important implication on the adsorption and reactivity of the O_2 species, as we will now show.

Adsorption energies, Bader charge analysis, and O–O bond distances for the interaction of an O_2 molecule with the Au_4 NP deposited on the different surface models under consideration are presented in Table 2.

As for CO adsorption, different coordination geometries have been considered but only the most stable ones are presented. In those configurations designed as “top” the O_2 molecule is interacting only with the gold NP atoms, while in those designed as “bottom”, the O_2 molecule is simultaneously coordinated to the gold NP and to the support surface (see Fig. 4).

This last configuration is the most stable in all surface models considered, with adsorption energies higher than -1.0 eV in the two dehydrated TiO_2 surface models (undoped and Y-doped) and higher than -2.0 eV in the hydrated Y-doped surface model when the Au NP sits on the O_v site. As the charge analysis shows, there is a direct relationship between the O_2 adsorption energy and the amount of charge transferred to the O_2 molecule. In all cases, the charge transfer takes place from the Au NP to the O_2 molecule and is larger when the Au NP is sitting on the O_v site. Moreover, this charge transfer has an important effect in the O_2 molecule activation: the electron

Table 1 Computed CO adsorption energies, Bader charge on Au_4 NP before CO adsorption (ini.) and after CO adsorption (fin.), CO bond distance and CO stretch vibrational frequency on different TiO_2 surface models

Model	E_{ads} eV	q_{Au} (ini.)	q_{Au} (fin.)	d_{CO} Å	ν_{CO} cm^{-1}
TiO_2	-1.38	$+0.01$	$+0.23$	1.153	2056
TiO_2 (H_2O)	-1.47	-0.04	$+0.22$	1.150	2086
Y- TiO_2	-1.30	-0.01	$+0.18$	1.150	2076
Y- $TiO_2 \cdot 3H_2O$ (Au)	-1.84	-0.14	$+0.24$	1.150	2081
Y- $TiO_2 \cdot 3H_2O$ (OH)	-1.46	-0.04	$+0.20$	1.148	2098

Table 2 Computed O_2 adsorption energies, Bader charge analysis, and O–O bond distance on different TiO_2 surface models

Model	Site	E_{ads} /eV	$q(O_2)$	d_{O-O} Å
TiO_2	Top	-0.32	-0.18	1.282
	Bottom	-1.22	-0.52	1.325
TiO_2 (H_2O)	Top	-0.12	-0.20	1.273
	Bottom	-0.70	-0.64	1.433
Y- TiO_2	Top	-0.06	-0.22	1.271
	Bottom	-1.09	-0.83	1.419
Y- $TiO_2 \cdot 3H_2O$ (Au)	Top	-0.53	-0.35	1.285
	Bottom	-2.20	-1.03	1.471
Y- $TiO_2 \cdot 3H_2O$ (OH)	Top	-0.35	-0.13	1.268
	Bottom	-0.41	-0.26	1.273

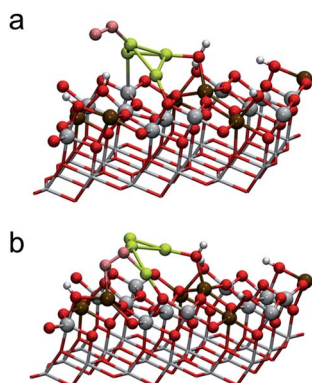


Fig. 4 Supercell models used for the O_2 adsorption on the Au_4 NP supported on the Y-doped hydrated TiO_2 (101) anatase surface. Atom colors: Ti, gray, O, red, Au, yellow, O_2 molecule, pink. (a) The O_2 molecule is interacting only with the gold NP. (b) The O_2 molecule is at the NP/support boundary.

density is transferred to antibonding orbitals, the O–O weakens and, correspondingly, the bond distance increases with respect to free O_2 as shown in Table 2. This effect is larger in the Y-doped models where we have a very reactive O_2^- species ready to interact with any incoming CO molecule. The data in Table 2 also allow us to shed light on the observed decrease in CO conversion in wet conditions (see Fig. 1). In the presence of water in the reactive flow some of the O_v sites will be occupied by hydroxyl groups, therefore displacing the Au NP from the O_v site. In these conditions (Y– $\text{TiO}_2 \cdot 3\text{H}_2\text{O}$ (OH) model) the O_2 adsorption energy significantly decreases to -0.41 eV and the charge transferred from the Au NP is also much lower ($0.26 e^-$). This results in an O_2 molecule only slightly perturbed, not strongly bound to the surface and not activated for reaction with CO. The values of adsorption energies for CO and O_2 suggest that if both gases are in contact with the surface, the CO and the O_2 are adsorbed on top and bottom positions respectively. The strong electronic transfer from the cluster to the O_2 results in a decrease in the donor capacity of the gold NP, being the σ -donation the most important component in the Au–CO bond. The low effect of the π -backdonation of the metallic particle to the CO molecule explains the high frequency of the observed band in DRIFT spectra, and it is consistent with the peroxide intermediate proposed by some authors for the CO oxidation reaction.¹⁴ To complete this analysis, we will, finally, examine the CO oxidation mechanism on a model Au_{10} NP deposited on Y-doped TiO_2 (101) surface.

The rate-limiting step in the CO oxidation reaction catalyzed by Au/oxide surface systems is the dissociation of the O_2 molecule.^{44,48} In principle, two mechanisms can be proposed: an O_2 dissociation taking place without help from the CO molecule; or, more commonly, an assisted mechanism where the CO molecule helps in the O_2 dissociation (Fig. 5). Regarding the first mechanism, our calculations show that the O_2 dissociation process is slightly endothermic by 0.10 – 0.24 eV, depending on the initial configuration considered. The O_2 activation is related to the charge transfer that takes place from the Au NP to the O_2 molecule adsorbed at the NP/surface

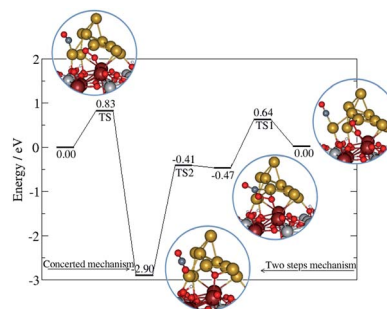


Fig. 5 Energy profiles for the CO oxidation reaction of Au_{10} /Y-doped TiO_2 (101) surface models. (Left) One step mechanism CO assisted O_2 dissociation. (Right) Two steps mechanism, with formation of a peroxo-type CO– O_2 complex (right). The insets show the most important structure on the reaction profiles.

interface previously discussed. However, the activation barrier for the process is quite high, 1.05 – 1.17 eV, and is similar to other values reported in the literature.^{49,50}

The CO assisted mechanism has been previously proposed in different reports with two variants. Remediakis *et al.*⁵¹ proposed a concerted mechanism in which the reaction between co-adsorbed CO and O_2 molecules, is accompanied by the rupture of the O–O bond and the CO_2 formation, all taking place in a single step. Molina *et al.*,⁵² and Hernandez *et al.*¹⁴ suggested a two-step mechanism, with formation of a peroxo-like intermediate complex $\text{O}_2 \cdots \text{CO}$ that subsequently leads to CO_2 , that desorbs, and an oxygen atom bound to the surface. We have explored both mechanisms starting from different initial configurations for the CO adsorption site and the reaction profiles are summarized in Fig. 5.

In both cases, the activation barriers are clearly smaller than that found for the direct O_2 dissociation mechanism (0.64 – 0.83 eV, see Fig. 5) and the two-step mechanism is clearly preferred. In the peroxo-like complex the O–O distance is further elongated up to 1.522 \AA , as a consequence of the electron donation that takes place from the CO molecule to the antibonding orbitals of the O_2 molecule. This additional destabilization of the O–O bond facilitates the O–O bond dissociation in a second step of lower activation energy (0.06 eV only). Thus the rate-determining step is now the attack of the O_2 molecule by the CO instead of the O–O bond dissociation.

Conclusions

In summary, by using catalytic activity measurements, characterization by DRIFTS and plane-wave pseudopotential density functional theory calculations, the role and dynamics of surface oxygen vacancies on the mechanism of the catalytic CO oxidation reaction by O_2 has been successfully investigated. Experimental data make clear that under dry and reactive flow conditions, the surface gets dehydroxylated and, simultaneously, the gold NPs are redispersed on the surface. The resulting solid is found to be more active for CO conversion in the second reaction cycle at low temperature as consequence of the observed redispersion of the Au NPs. The presence of water

in the reactive flow is found to inhibit the surface dehydroxylation, and no modifications were detected in a second cycle of reaction.

Employing density functional theory calculations and slab models of a Y-doped TiO₂ (101) anatase surface a microscopic understanding of the surface dynamics, the role of surface oxygen vacancies in the gold redispersion and on the activation of the O₂ molecule has been accomplished. It is found that while there should be a competition between the OH and the Au NP to occupy the surface oxygen vacancy sites, when the surface gets dehydrated the adsorption energy of gold NP on these sites notably increases. This explains the observed redispersion of the gold on the TiO₂-Y support under reaction conditions.

Moreover, our theoretical calculations predict a surface to Au charge transfer upon adsorption at the O_v site. A closer examination of the microscopic CO oxidation shows that upon CO adsorption, there is a charge reorganization inside the Au NP, resulting in a higher electron density at the Au NP/TiO₂ interface that play an essential role in the activation of the O₂ molecule. Upon O₂ molecule adsorption, a charge transfer to the O₂ antibonding orbitals takes place, resulting in a weakening of the O–O bond, manifested in a significant lengthening of the bond distance with respect to free O₂. This electronic transfer implies a high positive charge on the gold particle and justifies the appearance of the band at 2194 cm⁻¹ when CO and O₂ are in contact with the surface.

The reaction mechanism is found to proceed through the formation of a peroxo-like complex, where the O–O bond strength is further decreased. The rate-limiting step is found to be the formation of this peroxo-like complex, but with an energetic barrier significantly lower than for a direct O₂ dissociation mechanism previously proposed. The DFT analysis also show that when water is present in the reactive flow, some Au NP will be displaced from the O_v sites reducing the number of available sites for O₂ adsorption. At the same time the electron density transfer from the Au NP to the O₂ molecule is significantly reduced. Both facts explain the lower activity found for the catalysts under wet conditions.

Experimental

Synthetic procedures

The support was synthesized by a sol-gel method using titanium *tert*-butoxyde and yttrium nitrate as metallic precursors. The used hydrolysis agent was a mixture H₂O/NH₃ (28.5/1 ratio) and the solvent 1-butanol. The excess of solvent was eliminated by Soxhlet solid-liquid extraction and the obtained solid was calcined at 300 °C for 2 h. The incorporation of 1 wt% of gold to the support was carried out using chloroauric acid (ALDRICH) as metallic source by a deposition-precipitation method. The pH of a solution of the acid precursor was adjusted to 7 by adding NaOH 0.1 M, then, the support was added and the solution maintained at constant temperature during 3 hours. Finally, the solid was washed until Cl-disappearance and the solid dried and calcined for 2 h at 300 °C. The procedure of preparation of both support and catalyst are detailed elsewhere.³⁴

Characterization

The BET specific surface area of the solid was determined by N₂ adsorption at liquid nitrogen temperature in a Micromeritics ASAP 2010 apparatus. The samples degasification was carried out at 150 °C for 2 hours in vacuum. The solid structure was studied by XRD using a Siemens Kristalloflex D-501 diffractometer working with Cu-K α radiation ($\lambda = 1.5404 \text{ \AA}$) in continuous scan mode over a 2θ range of 20–80° using a step size of 0.05° and a step time of 1.0 s. The chemical composition was determined by X-ray fluorescence (XRF) with a Siemens SRS 3000 sequential spectrophotometer equipped with a rhodium tube. The measurements were performed onto pressed pellets (sample included 10 wt% of wax).

Catalytic activity

A conventional continuous flow U-shaped glass reactor working at atmospheric pressure was used to measure the catalytic activity of the solid. A thermocouple in contact with the catalytic bed (about 80 mg of solid placed between two plugs of glass wool) assures the right measurement and the correct control of the temperature during the light-off experiments. A set of mass flow controllers (Bronkhorst) were used to prepare the activation (21% O₂ in He) and reaction (3.4% CO and 21% O₂, balanced by He) flows at a total flow rate of 42 mL min⁻¹. For the tests in wet conditions, the reactive flow was forced to pass through a water saturator at room temperature before to be sent to the reactor. In these conditions, the water content in the reactive mixture is about 2 vol%. The *in situ* activation of the solids was carried out at 300 °C (10 °C min⁻¹) during 1 hour. Then, the temperature was decreased to room temperature and the light-off curves started. The gaseous flow becoming from the reactor was analyzed by a BalzersThermostarbench top mass spectrometer controlled by the software BalzersQuadstar 422 with capabilities for quantitative analysis. The gases, 99.997% pure, were provided by Air Liquide.

DRIFTS-MS measurements

Studies of the surface under reactive conditions were performed in a DRIFT (Diffuse Reflectance Infrared Fourier Spectroscopy) cell coupled to a mass spectrometer (BalzersThermostar) in similar conditions (gas flow and temperature) to those used in the classical reactor. The DRIFT chamber (Spectra-Tech 101) with SeZn windows was coupled to a Thermo Nicolet Nexus infrared spectrometer with KBr optics and a MCT/B detector working at liquid nitrogen temperature. Spectra (64 scans per spectrum and 4 cm⁻¹) were recorded every 2 minutes during the reaction and the gas mixture becoming from the cell-reactor was continuously analyzed by mass spectrometry.

Theoretical models and computational details

To model the extended nature of these surfaces, periodic three-dimensional DFT calculations were carried out using the VASP 4.6 code^{52–55} with the projector augmented wave (PAW) method.^{56,57} In these calculations, the energy was obtained using the generalized gradient approximation (GGA) implementation

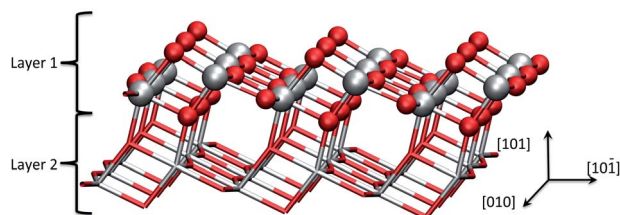


Fig. 6 The 3×3 supercell model of a TiO_2 (110) anatase surface used in this study. Atoms colors: Ti, gray, O, red.

of DFT proposed by Perdew *et al.*⁵⁸ and the electronic states were expanded using plane wave basis set with a cutoff of 400 eV. A spin-polarized formalism has been used when we were dealing with single gold adatoms or when the system included the O_2 molecule. Forces on the ions were calculated through the Hellmann–Feynman theorem, including the Harris–Foulkes correction to forces.⁵⁹ Iterative relaxation of the atomic positions was stopped when the forces on the atoms were less than 0.05 eV \AA^{-1} .

Anatase TiO_2 (101) slab models with two O–Ti–O trilayers and 14 \AA vacuum width were used to describe the support, as previous experimental and theoretical studies have shown that the (101) plane is the most stable low index surface of anatase TiO_2 .^{60,61} Given that numerous initial geometries for CO and O_2 adsorption were to be explored with different gold aggregates and with or without the simultaneous presence of OH at the surface, the width of the slab model was limited to two O–Ti–O trilayers, as indicated. For the initial studies of CO and O_2 adsorption on Au adatoms and Au_4 nanoparticles (NP) the supercell dimensions were 3×3 in the [010] and $[10\bar{1}]$ directions, respectively (see Fig. 6).

In this model, following the conclusions of previous work³⁴ and to have dopant loadings similar to those experimentally found, six Ti atoms were substituted by Y atoms and three oxygen vacancies (O_v) sites were created. To examine the CO oxidation reaction mechanism a larger supercell of dimensions 4×3 in the [010] and $[10\bar{1}]$ directions was used. Eight Ti atoms were substituted in this model by Y atoms and four O_v sites were created. A large Au_{10} NP, similar in size to the smallest gold NP experimentally characterized⁶² was deposited on this surface. In all cases the Brillouin zone was sampled at the Γ point. To analyze the charge transfer upon adsorption a Bader type analysis was performed.^{63–65} Up to four different models of the anatase TiO_2 (101) surface were used: undoped and dehydrated, designed as TiO_2 in the data tables, undoped and hydrated, shown as $\text{TiO}_2 \cdot \text{H}_2\text{O}$, Y-doped dehydrated mode, shown as Y– TiO_2 , and Y-doped and hydrated, designed as Y– $\text{TiO}_2 \cdot \text{H}_2\text{O}$. From this last surface, and for the adsorption of CO an O_2 molecules, two different models were derived, depending on whether the Au NP was (indicated by Au at the model denomination in the data tables) or was not (OH) occupying an O_v site.

Acknowledgements

This work was funded by the Ministerio de Economía y Competitividad (Spain) and the EU FEDER program, grants

MAT2012-31526 and CSD2008-0023 and project ENE2012-37431-C03-01. Computational resources were provided by the Barcelona Supercomputing Center/Centro Nacional de Supercomputación (Spain).

Notes and references

- 1 *Nanoparticles and Catalysis*, ed. A. Didier, Wiley-VCH, 2008, ISBN: 978-3-527-31572-7.
- 2 G. C. Bond and D. T. Thompson, *Gold Bull.*, 2000, **33**, 41–51.
- 3 M. C. Kung, R. J. Davis and H. H. Kung, *J. Phys. Chem. C*, 2007, **111**, 11767–11775.
- 4 M. Haruta, *Catal. Today*, 1997, **36**, 153–166.
- 5 M. Haruta, *CATTECH*, 2002, **6**, 102–115.
- 6 J. B. Park, J. Graciani, J. Evans, D. Stacchiola, S. Ma, P. Liu, A. Nambu, J. F. Sanz, J. Hrbek and J. A. Rodríguez, *Proc. Natl. Acad. Sci. U. S. A.*, 2009, **106**, 4975–4980.
- 7 J. A. Rodríguez, *Catal. Today*, 2011, **160**, 3–10.
- 8 O. H. Laguna, M. A. Centeno, G. Arzamendi, L. M. Gandía, F. Romero-Sarria and J. A. Odriozola, *Catal. Today*, 2010, **157**, 155–159.
- 9 O. H. Laguna, M. A. Centeno, F. Romero-Sarria and J. A. Odriozola, *Catal. Today*, 2011, **172**, 118–123.
- 10 H. Y. Kim, H. M. Lee and G. Henkelman, *J. Am. Chem. Soc.*, 2012, **134**, 1560–1570.
- 11 M. Ojeda, B. Z. Zhan and E. Iglesia, *J. Catal.*, 2012, **285**, 92–102.
- 12 F. Romero-Sarria, M. I. Domínguez, M. A. Centeno and J. A. Odriozola, *Appl. Catal., B*, 2011, **107**, 268–273.
- 13 K. Qian, W. Zhang, H. Sun, J. Fang, B. He, Y. Ma, Z. Jiang, S. Wei, J. Yang and W. Huang, *J. Catal.*, 2011, **277**, 95–103.
- 14 N. C. Hernández, J. F. Sanz and J. A. Rodríguez, *J. Am. Chem. Soc.*, 2006, **128**, 15600–15601.
- 15 S. A. C. Carabineiro, A. M. T. Silva, G. Drazic, P. B. Tavares and J. L. Figueiredo, *Catal. Today*, 2010, **154**, 21–30.
- 16 M. C. Saint-Lager, I. Laoufi, A. Bailly, O. Robach, S. Garaudee and P. Dolle, *Faraday Discuss.*, 2011, **152**, 253–265.
- 17 M. Valden, X. Lai and D. W. Goodman, *Science*, 1998, **281**, 1647–1650.
- 18 M. Chen and D. W. Goodman, *Science*, 2004, **306**, 252–255.
- 19 J. Guzman and B. C. Gates, *J. Phys. Chem. B*, 2002, **106**, 7659–7665.
- 20 J. Guzman and B. C. Gates, *J. Am. Chem. Soc.*, 2004, **126**, 2672–2673.
- 21 Y. Guan, D. A. J. M. Ligthart, O. Pirgon-Galin, J. A. Z. Pieterse, R. A. van Santen and E. J. M. Hensen, *Top. Catal.*, 2011, **54**, 424–438.
- 22 F. Moreau and G. C. Bond, *Catal. Today*, 2006, **114**, 362–368.
- 23 G. J. Hutchings, M. S. Hall, A. F. Carley, P. Landon, C. J. Solsona, A. Kiely, M. Herzing, J. A. Makkee, A. Moulijn, B. E. Overweg, J. C. Fierro-Gonzalez, J. Guzman and B. C. Gates, *J. Catal.*, 2006, **242**, 71–81.
- 24 N. Weiher, E. Bus, L. Delannoy, C. Louis, D. E. Ramaker, J. T. Miller and J. A. van Bokhoven, *J. Catal.*, 2006, **240**, 100–107.
- 25 T. Minato, T. Susaki, S. Shiraki, H. S. Kato, M. Kawai and K. I. Aika, *Surf. Sci.*, 2004, **566**, 1012–1017.

- 26 C. Ruggiero and P. Hollins, *J. Chem. Soc., Faraday Trans.*, 1996, **92**, 4829–4834.
- 27 G. C. Bond and D. T. Thompson, *Catal. Rev. Sci. Eng.*, 1999, **41**(3&4), 319–388.
- 28 M. M. Schubert, S. Hackenberg, A. C. van Veen, M. Muhler, V. Plzak and R. J. Behm, *J. Catal.*, 2001, **113**, 113–122.
- 29 D. Widmann, Y. Liu, F. Schüth and R. J. Behm, *J. Catal.*, 2010, **276**, 292–305.
- 30 M. I. Domínguez, F. Romero-Sarria, M. A. Centeno and J. A. Odriozola, *Appl. Catal., B*, 2009, **87**, 245–251.
- 31 W. Y. Hernández, M. A. Centeno, F. Romero-Sarria and J. A. Odriozola, *J. Phys. Chem. C*, 2009, **113**, 5629–5635.
- 32 J. Graciani, A. Nambu, J. Evans, J. A. Rodríguez and J. F. Sanz, *J. Am. Chem. Soc.*, 2008, **130**, 12056–12063.
- 33 F. Romero-Sarria, T. L. M. Martínez, M. A. Centeno and J. A. Odriozola, *J. Phys. Chem. C*, 2007, **111**, 14469–14475.
- 34 J. J. Plata, A. M. Márquez, J. F. Sanz, R. S. Avellaneda, F. Romero-Sarria, M. I. Domínguez, M. A. Centeno and J. A. Odriozola, *Top. Catal.*, 2011, **54**, 219–228.
- 35 A. Simakov, I. Tuzovskaya, A. Pestryakov, N. Bogdanchikova, V. Gurin, M. Avalos and M. H. Fariás, *Appl. Catal., A*, 2007, **331**, 121–128.
- 36 M. Daté and M. Haruta, *J. Catal.*, 2001, **201**, 221–224.
- 37 M. A. Bollinger and M. A. Vannice, *Appl. Catal., B*, 1996, **8**, 417–443.
- 38 F. Boccuzzi and A. Chiorino, *J. Phys. Chem. B*, 2000, **104**, 5414–5416.
- 39 K. Hadjiivanov and G. Vayssilov, *Adv. Catal.*, 2000, **47**, 307–511.
- 40 T. Risse, S. Shaikhutdinov, N. Nilius, M. Sterrer and H.-J. Freund, *Acc. Chem. Res.*, 2008, **41**, 949–956.
- 41 M. Sterrer, M. Yulikov, E. Fischbach, M. Heyde, H. P. Rust, G. Pacchioni, T. Risse and H. Freund, *Angew. Chem., Int. Ed.*, 2006, **45**, 2630–2632.
- 42 H. Willner and F. Aubke, *Inorg. Chem.*, 1990, **29**, 2195.
- 43 J. A. Toledo-Antonio, S. Capula, M. A. Cortés-Jácome, C. Ángeles-Chávez, E. López-Salinas, G. Ferrat, J. Navarrete and J. Escobar, *J. Phys. Chem. C*, 2007, **111**, 10799–10805.
- 44 M. Primet, P. Pichat and M. V. Mathieu, *J. Phys. Chem.*, 1971, **75**, 1216–1220.
- 45 T. Żmijewski, M. Mioduska and J. Pysiak, *J. Therm. Anal. Calorim.*, 2000, **60**, 247–255.
- 46 S. T. Daniells, A. R. Overweg, M. Makkee and J. A. Moulijn, *J. Catal.*, 2005, **230**, 52.
- 47 A. Márquez, J. Graciani and J. F. Sanz, *Theor. Chem. Acc.*, 2010, **126**, 265–273.
- 48 C. Zhang, B. Yoon and U. Landman, *J. Am. Chem. Soc.*, 2007, **129**, 2228–2229.
- 49 A. Tilocca, C. Di Valentin and A. Selloni, *J. Phys. Chem. B*, 2005, **109**, 20963.
- 50 S. Chretien and H. Metiu, *J. Chem. Phys.*, 2008, **129**, 074705.
- 51 I. N. Remediakis, N. López and J. K. Nørskov, *Angew. Chem., Int. Ed.*, 2005, **44**, 1824–1826.
- 52 L. M. Molina and B. Hammer, *Appl. Catal., A*, 2005, **291**, 21.
- 53 G. Kresse and J. Hafner, *Phys. Rev. B: Condens. Matter Mater. Phys.*, 1993, **47**, 558–561.
- 54 G. Kresse and J. Furthmüller, *Comput. Mater. Sci.*, 1996, **6**, 15–50.
- 55 G. Kresse and J. Furthmüller, *Phys. Rev. B: Condens. Matter Mater. Phys.*, 1996, **54**, 11169–11186.
- 56 P. E. Blöchl, *Phys. Rev. B: Condens. Matter Mater. Phys.*, 1994, **50**, 17953–17959.
- 57 G. Kresse and D. Joubert, *Phys. Rev. B: Condens. Matter Mater. Phys.*, 1999, **59**, 1758–1775.
- 58 J. P. Perdew, J. A. Chevary, S. H. Vosko, K. A. Jackson, M. R. Pederson, D. J. Singh and C. Fiolhais, *Phys. Rev. B: Condens. Matter Mater. Phys.*, 1992, **46**, 6671–6687.
- 59 J. Harris, *Phys. Rev. B: Condens. Matter Mater. Phys.*, 1985, **31**, 1770.
- 60 U. Diebold, *Surf. Sci. Rep.*, 2003, **48**, 53–229.
- 61 M. Lazzeri, A. Vittadini and A. Selloni, *Phys. Rev. B: Condens. Matter Mater. Phys.*, 2001, **63**, 155409.
- 62 C. Chan Sze and M. A. Barteau, *Langmuir*, 2005, **21**, 5588–5595.
- 63 G. Henkelman, A. Arnaldsson and H. Jonsson, *Comput. Mater. Sci.*, 2006, **36**, 354–360.
- 64 E. Sanville, S. D. Kenny, R. Smith and G. Henkelman, *J. Comput. Chem.*, 2007, **28**, 899–908.
- 65 R. Bader, *Atoms in Molecules: A Quantum Theory*, Oxford University Press, 1990.